Nanoscale Research Letters

NANO EXPRESS Open Access

$MoSe_2$-Ni_3Se_4 Hybrid Nanoelectrocatalysts and Their Enhanced Electrocatalytic Activity for Hydrogen Evolution Reaction

Pengyuan Wu, Gangyong Sun, Yuanzhi Chen*, Wanjie Xu, Hongfei Zheng, Jin Xu*, Laisen Wang and Dong-Liang Peng

Abstract

Combining $MoSe_2$ with other transition metal dichalcogenides to form a hybrid nanostructure is an effective route to enhance the electrocatalytic activities for hydrogen evolution reaction (HER). In this study, $MoSe_2$-Ni_3Se_4 hybrid nanoelectrocatalysts with a flower-like morphology are synthesized by a seed-induced solution approach. Instead of independently nucleating to form separate nanocrystals, the Ni_3Se_4 component tends to nucleate and grow on the surfaces of ultrathin nanoflakes of $MoSe_2$ to form a hybrid nanostructure. $MoSe_2$–Ni_3Se_4 hybrid nanoelectrocatalysts with different Mo:Ni ratios are prepared and their HER catalytic activities are compared. The results show that the HER activities are affected by the Mo:Ni ratios. In comparison with pure $MoSe_2$, the $MoSe_2$-Ni_3Se_4 hybrid nanoelectrocatalysts having a Mo:Ni molar ratio of 2:1 exhibit enhanced HER properties with an overpotential of 203 mV at 10 mA/cm^2 and a Tafel slope of 57 mV per decade. Improved conductivity and increased turnover frequencies (TOFs) are also observed for the $MoSe_2$-Ni_3Se_4 hybrid samples.

Keywords: Hydrogen evolution reaction, $MoSe_2$, Electrocatalysis, Nickel selenides, Hybrid nanostructure

Introduction

Traditional fossil fuels are the main energy sources in our society; however, they are non-renewable and unsustainable, and are causing serious pollution to environment. Among alternative energies, hydrogen energy has been regarded as one of the most promising clean energies because of its ultrahigh energy density [1]. Up to now, the large-scale production of hydrogen is still mainly from fossil fuel sources [2]. Coal gasification and methane steam reforming industrially produce 95% of hydrogen [3]. Hydrogen evolution reaction (HER) has been considered as a promising route to generate high-purity hydrogen [1, 4, 5]. However, the best electrocatalysts for HER in acidic media are still Pt-based and other noble metal materials [6]. Due to their scarcity and high cost, the Pt-based materials are not suitable to be applied in large-scale hydrogen evolution [7].Transition metal dichalcogenides (TMDs), like MoS_2, $MoSe_2$, WS_2, and WSe_2, have received intensive attentions owing to their excellent electrochemical properties and earth abundant nature. As a typical layered TMD semiconducting material, $MoSe_2$ has a similar structure to graphite, and is formed by Se–Mo–Se layers that are bonded via the van der Waals forces. In addition, $MoSe_2$ is more metallic than MoS_2, and has a lower Gibbs free energy of the hydrogen adsorption onto the edge of $MoSe_2$ than MoS_2, which leads to a higher adsorption of hydrogen [8]. On this account, $MoSe_2$ and its hybrids have captured much attention as electrocatalysts for HER.

It is well known that only active sites are effective for HER. For two-dimensional layered nanostructures like TMD nanosheets, the active sites for HER are located along the nanosheet edges [9], whilst the basal surfaces are inert. The conductivity of electrocatalysts is also an important issue for HER. As a kind of semiconductor, the poor

* Correspondence: yuanzhi@xmu.edu.cn; xujinmse@xmu.edu.cn
Department of Materials Science and Engineering, Collaborative Innovation Center of Chemistry for Energy Materials, College of Materials, Xiamen University, Xiamen 361005, China

electron transport ability of $MoSe_2$ compared to noble metals is still limiting its performance in HER [10]. Therefore, the general strategies for improving the activity of TMD catalysts are to enhance the electrical conductivity [11, 12] and increase the active site numbers [12–14]. Meanwhile, designing hybrid structures by integrating different types of semiconductive materials especially TMDs with a preferred orientation is considered to be an important approach to tuning the electronic properties of semiconductive materials [15–17]. Hybrid nanostructures with efficient heterointerfaces can promote rapid interfacial charge transfer, which is pivotal to the electrochemical reactions [18]. Besides, it is well known that three elementary steps, i.e., adsorption, reduction, and desorption, are required to generate hydrogen during the electrochemical reactions [19]. One of the superiority for hybrid materials composing of different chemical components is that they may break through the limitation that many single-component catalysts are not effective for all the three intermediate reaction processes. Recently, some researchers have integrated Ni-based catalysts with $MoSe_2$ in various morphologies by using different methods to achieve enhanced HER performances [15, 18, 20]. The combination of $MoSe_2$ with Ni selenides to form a hybrid structure may utilize the synergistic effect that arises from the interaction between two heterogeneous components to achieve enhanced electrocatalytic activity. For example, a DFT calculation indicated that the $MoS_{2(1-x)}Se_{2x}/NiSe_2$ had much lower hydrogen adsorption Gibbs free energy on (100) and (110) planes than pure $MoS_{2(1-x)}Se_{2x}$, which could result in higher coverage of hydrogen at the active sites and therefore achieved outstanding electrocatalytic performances [21].

Herein, we attempt to prepare hybrid nanoelectrocatalysts by growing Ni_3Se_4 on the surfaces of flower-like $MoSe_2$ seeds which are synthesized via a colloidal method reported in our previous study [22]. Such a seed-induced growing approach offers a facile means to build various TMD hybrid nanostructures. The reason why we select Ni_3Se_4 as the hybrid component is that Ni_3Se_4 has a higher electrical conductivity than other nickel selenides [23]. In order to investigate the influences of Ni_3Se_4 on catalyst's activity and find out the best composition ratio, we systematically modulated the content of Ni_3Se_4 and $MoSe_2$, and found that the incorporation of moderate content Ni_3Se_4 into the $MoSe_2$–Ni_3Se_4 hybrid systems can improve the HER performances. Our results suggest that the construction of a hybrid nanostructure of $MoSe_2$–Ni_3Se_4 is an effective approach to improve the HER performances of pure $MoSe_2$.

Methods/Experimental

Synthesis of $MoSe_2$–Ni_3Se_4 Hybrid Nanoelectrocatalysts

The synthesis of $MoSe_2$–Ni_3Se_4 hybrid nanoelectrocatalysts involved two steps. In the first step, $MoSe_2$ seeds were synthesized according to the method reported in our previous study [22]. Briefly, 10 mL of oleic acid (OA, 85%, Aladdin Bio-Chem Technology Co., Ltd.) and 0.4 mmol of molybdenum hexacarbonyl ($Mo(CO)_6$, 98%, J&K Scientific Ltd.) were mixed and heated up to 85 °C slowly in argon gas. Subsequently, the temperature of the mixed solution was increased to 200 °C and 6.7 mL of pre-prepared solution containing 1-octadecene (ODE, 90%, Aladdin Bio-Chem Technology Co., Ltd.) and Se (99.999%, J&K Scientific Ltd.) with a Se concentration of 0.15 mmol/mL was injected into the reaction solution using an injecting speed of 0.5 mL/min. When the injection was completed, the reaction was further maintained for 30 min to generate $MoSe_2$ seeds. In the next step, the reaction temperature was increased to 300 °C, and a mixture of 3.3 mL solution of ODE and Se, and nickel(II) acetylacetonate ($Ni(acac)_2$, 0.2 mmol, 96%, J&K Scientific Ltd.) was injected into the reaction mixtures and kept at 300 °C for 30 min. After cooling down to room temperature, the reaction products were washed with ethanol and hexane, and then undergoing drying at room temperature. The synthesized sample was labeled as Mo2Ni1, denoting that the molar ratio of Mo:Ni in $MoSe_2$–Ni_3Se_4 hybrid samples is 2:1. Other $MoSe_2$–Ni_3Se_4 nanohybrid samples with different Mo to Ni ratios were synthesized using the same procedure except that different qualities of mixtures of Ni and Se sources were added in the reaction.

Characterization

The crystalline phase was characterized using by an X-ray diffractometer (Bruker D8-Advance). Transmission electron microscopy (TEM) images were obtained using a JEM-2100 transmission electron microscope. High-angle annular dark-field (HAADF) imaging and corresponding elemental mapping were performed with a TECNAI F-30 transmission electron microscope. Scanning electron microscopy (SEM) images were acquired using a SU-70 scanning electron microscope. X-ray photoelectron spectroscopy (XPS) data were obtained via a spectrometer (PHI QUANTUM 2000) with Al Kα source.

Electrochemical Tests

The electrochemical tests were conducted in a standard testing system containing a reference electrode of Ag/AgCl, a graphite rod counter electrode and a glass-carbon working electrode which were connected to an Autolab 302N electrochemical workstation that used H_2SO_4 (0.5 M) as electrolyte. To prepare electrocatalyst ink, the synthesized electrocatalysts (4 mg), Ketjenblack carbon black (0.5 mg), and Nafion solution (30 μL) were mixed with ethanol-water solution (1 mL) with an ethanol content of 20 vol%. The mixtures were then

ultrasonicated for 30 min. Finally, 5 μL of ink (containing about 20 μg electrocatalysts) was deposited on the glassy carbon electrode to form a film that had a loading of about 0.286 mg/cm^2 and dried at room temperature. The polarization curves were obtained by using a scan rate of 2 mV s^{-1} at 25 °C from 0.2 to − 0.6 V (versus reversible hydrogen electrode (RHE)). The electrochemical impedance spectroscopy (EIS) data were obtained at frequencies ranging from 0.01 Hz to 100 kHz at − 260 mV. The cyclic voltammetry (CV) test was carried out to obtain the double-layer capacitance (non-Faradaic potential) from 0.1 to 0.2 mV and to calculate the effective surface area of electrode.

Results and Discussion

The synthesis of $MoSe_2$–Ni_3Se_4 hybrid nanoelectrocatalysts is based on a seed-induced strategy in which nanoscale Ni_3Se_4 grows in situ on the pre-formed $MoSe_2$ seeds (Fig. 1). In the first step, $MoSe_2$ seeds were synthesized via the reaction between Mo precursor ($Mo(CO)_6$) and Se in the presence of OA in ODE at 200 °C in which process ultrathin $MoSe_2$ nanoflakes which were formed during the heating process were further self-assembled into flower-like $MoSe_2$ particles [22]. The flower-like morphology with large surface area may facilitate the dispersion and intimate interaction of the second component [24]. After the temperature reached at 300 °C, the solution containing $Ni(acac)_2$ and ODE-Se was rapidly injected into the hot reaction mixtures containing $MoSe_2$ seeds. At this stage, Ni_3Se_4 nucleates and grows on the surface of $MoSe_2$ nanoflakes to form $MoSe_2$–Ni_3Se_4 hybrid nanostructures. This facile synthetic strategy is effective for the synthesis of $MoSe_2$–Ni_3Se_4 hybrid nanoelectrocatalysts with different Mo:Ni ratios under similar experimental conditions and may be employed to build other $MoSe_2$-based hybrid nanoelectrocatalysts.

Figure 2 compares the XRD patterns of pure $MoSe_2$ and $MoSe_2$–Ni_3Se_4 hybrid samples. The diffraction peaks of pure $MoSe_2$ sample are in accordance with hexagonal $MoSe_2$ (PDF# 29-0914) while the $MoSe_2$–Ni_3Se_4 hybrid samples with different Mo:Ni ratios exhibit the combinational peaks of hexagonal $MoSe_2$ and monoclinic Ni_3Se_4 (PDF# 13-0300). As the content of Ni precursor added increases, the peak intensity of Ni_3Se_4 in the XRD patterns also increases, which indicate that the concentration of Ni_3Se_4 in the $MoSe_2$–Ni_3Se_4 hybrid nanoelectrocatalysts increases too. Therefore, the content of Ni_3Se_4 in the $MoSe_2$–Ni_3Se_4 hybrid nanoelectrocatalysts can be tuned by controlling the content of the Ni precursor added. The SAED analyses (Additional file 1: Figure S1) also reveal the co-existence of hexagonal $MoSe_2$ and monoclinic Ni_3Se_4, which confirm the XRD results. As the content of

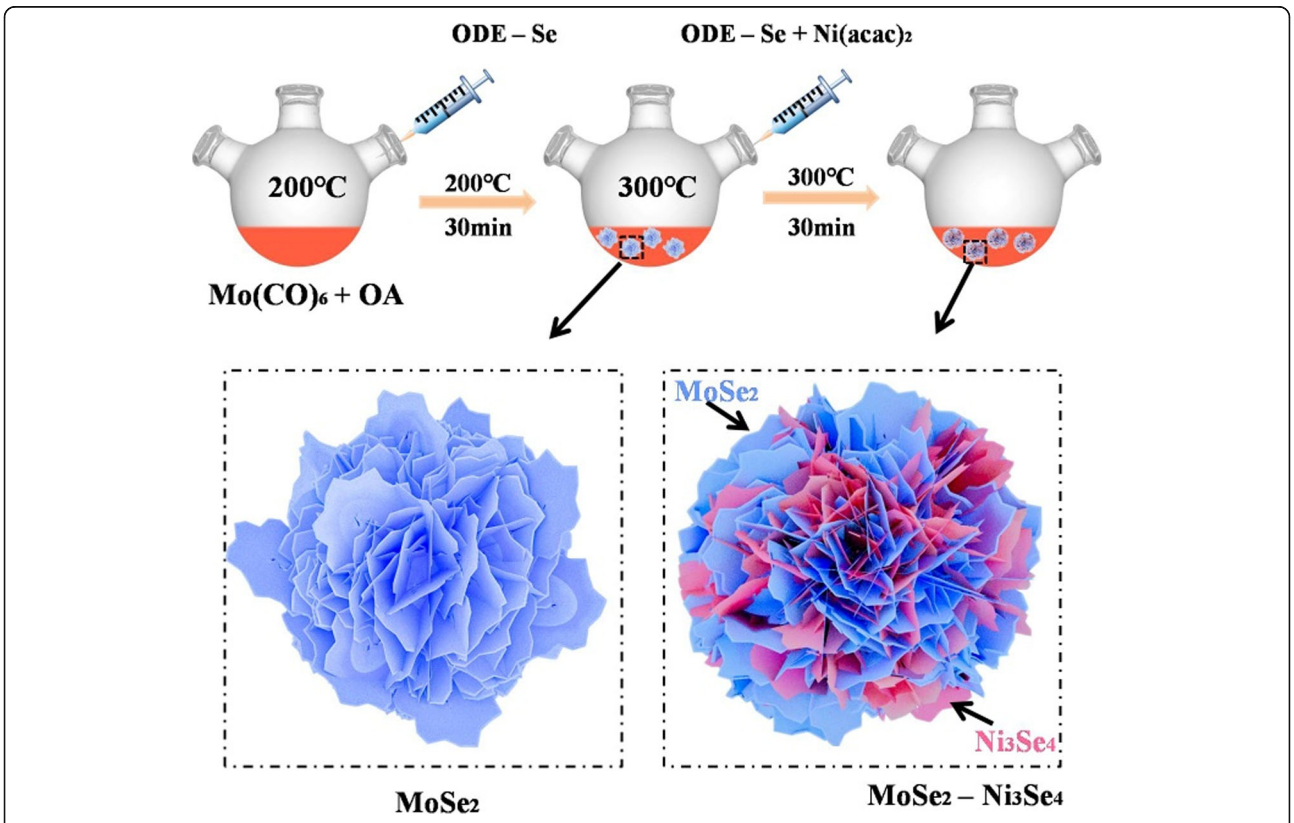

Fig. 1 Schematic diagram of the formation of $MoSe_2$–Ni_3Se_4 hybrid nanoelectrocatalysts

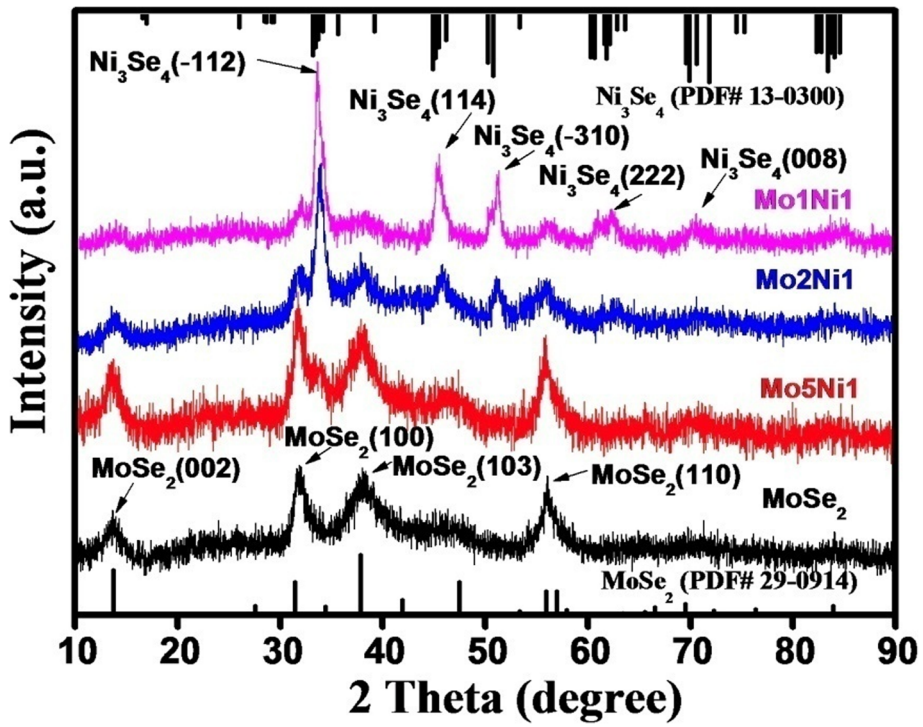

Fig. 2 XRD patterns of pure $MoSe_2$ and $MoSe_2$–Ni_3Se_4 hybrid samples with different Mo:Ni ratios. Reference patterns of bulk $MoSe_2$ and Ni_3Se_4 are also included

Ni precursor added increases, the diffraction rings belonging to Ni_3Se_4 also become prominent, demonstrating that the relative content of Ni_3Se_4 component in $MoSe_2$–Ni_3Se_4 hybrid nanoelectrocatalysts increases too.

The morphology of as-prepared samples was analyzed by SEM and TEM. The pure $MoSe_2$ possesses a flower-like morphology that has a size ranging from 100 to 200 nm (Additional file 1: Figure S2). Upon incorporating Ni_3Se_4, it can be distinctly seen that the petals of nanoflowers begin to become thicker (Fig. 3), and the flower-like morphology tends to disappear gradually with increasing the Ni_3Se_4 content. High-resolution TEM (HRTEM) analyses (Fig. 4a, b) on Mo2Ni1 sample reveal two types of evident lattice fringes: the one having an interplanar spacing of 0.64 nm corresponds to the (002) plane of $MoSe_2$ [25], and the one with an interplanar spacing of 0.27 nm agrees well with the (−112) plane of Ni_3Se_4. The result confirms the presence of both $MoSe_2$ and Ni_3Se_4 components in a hybrid nanostructure, and the main surfaces of nanoflower petals are constituted by the {001} facets of $MoSe_2$. In addition, the two different lattice fringes are roughly in parallel, indicating that Ni_3Se_4 may grow on the {001} facets of $MoSe_2$ along the c-axis of $MoSe_2$.

Energy-dispersive X-ray spectroscopy (EDS) elemental maps along with the HAADF image (Fig. 4**d**–**f**) confirm the presence of Se, Ni and Mo. However, the spatial distribution of Mo and Ni is slightly different. Mo is basically distributed homogeneously in the nanoflower, whereas Ni tends to concentrate near the petals of the nanoflower, which indicate that Ni_3Se_4 should grow on $MoSe_2$ petals. The covering of thicker Ni_3Se_4 layers on the $MoSe_2$ may block the active sites of $MoSe_2$ and eventually leads to declined HER performances. Besides to the injected amount of Ni and Se sources, the injection rate also affects the morphology of $MoSe_2$–Ni_3Se_4 hybrid nanostructure. When a smaller injection rate (1.65 mL/min) of Ni and Se sources was used, the products turned out to have an inhomogeneous morphology (Additional file 1: Fig. S3). This indicates that the formation of $MoSe_2$–Ni_3Se_4 hybrid nanostructure is also a kinetically controlled process.

XPS analyses (Fig. 5a–d) further verify the presence of Mo, Ni, and Se in the hybrid sample (take Mo2Ni1 as a typical example). For Se 3d regions (Fig. 5b), the two peaks at 54.75 and 55.75 eV are assigned to Se $3d_{5/2}$ and Se $3d_{3/2}$, respectively, which indicates that the oxidation state for Se at is − 2 [26]. The obvious peak at 59.37 eV suggests that the Se species at surfaces has been oxidized [20, 26]. In Fig. 5c, two peaks located at 229.37 and 232.50 eV are assigned to Mo $3d_{5/2}$ and $3d_{3/2}$, respectively, which indicate the +4 oxidation state of Mo [8, 11, 26]. In Fig. 5d, the Ni 2p peaks are clearly present, and the peaks at 856.62 and 874.12 eV agree well with Ni $2p_{3/2}$ and Ni $2p_{1/2}$, respectively. The two satellite peaks

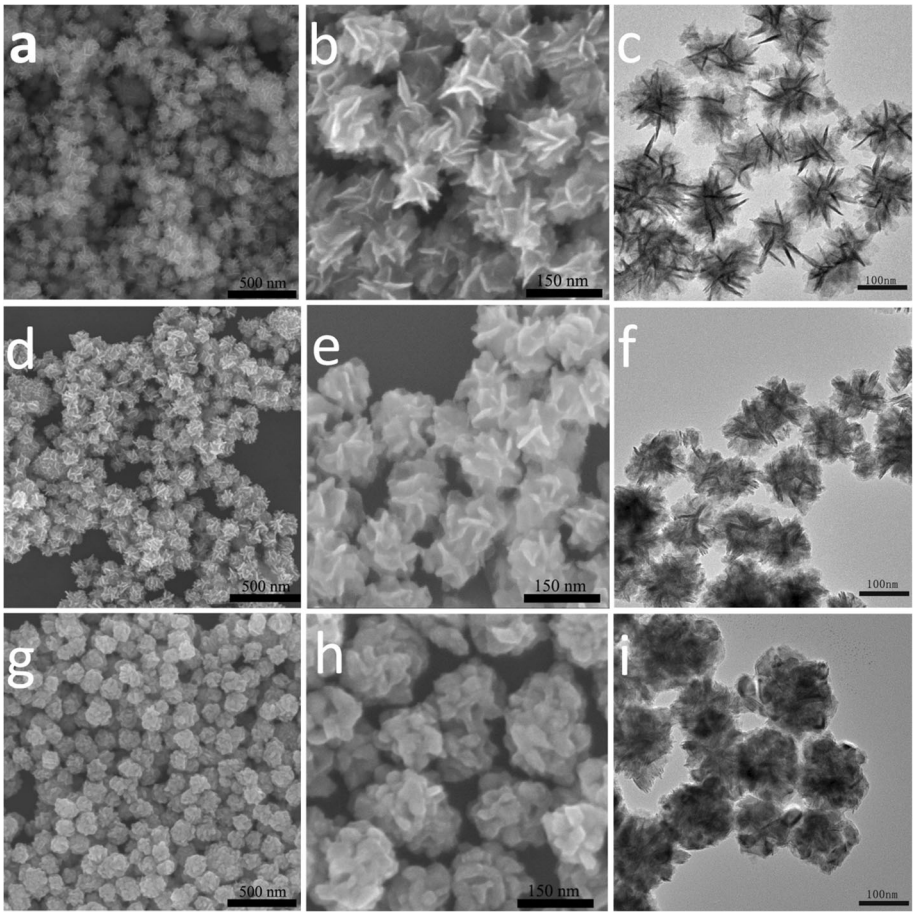

Fig. 3 SEM images (**a**, **b**, **d**, **e**, **g**, and **h**) and TEM images (**c**, **f**, and **i**) of Mo5Ni1 (**a**–**c**), Mo2Ni1 (**d**–**f**) and Mo1Ni1 (**g**–**i**) samples

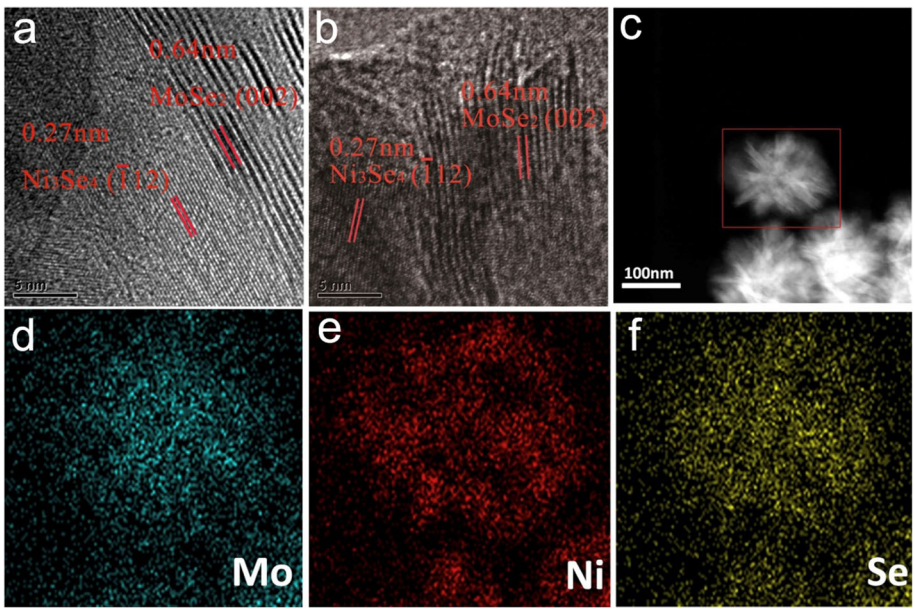

Fig. 4 HRTEM images (**a** and **b**), HAADF image (**c**) and elemental maps (**d**–**f**) of Mo2Ni1 sample

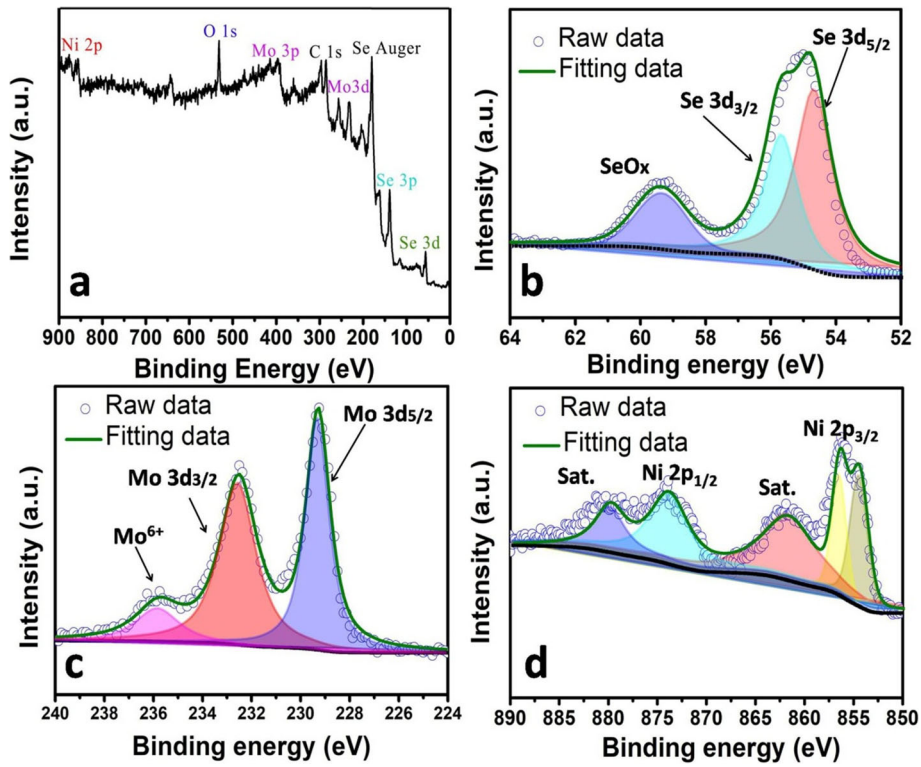

Fig. 5 XPS spectra of Mo2Ni1 sample. **a** is the survey spectrum. **b**), **c**, and **d** show the expanded spectra of Se, Mo, and Ni, respectively

at 861.87 and 880.37 eV suggest that Ni is in the oxidation state close to + 2 [27].

The formation mechanism of $MoSe_2$–Ni_3Se_4 hybrid nanostructure can be understood from the above characterization results. The flower-like $MoSe_2$ seeds play an important role in inducing the formation of Ni_3Se_4 on the surfaces of $MoSe_2$. At the reaction temperature of 300 °C, $Ni(acac)_2$ is easily to decompose to react with Se to form Ni_3Se_4. The surfaces of $MoSe_2$ can act as heterogeneous-nucleation sites to induce the nucleation of Ni_3Se_4. Obviously such a heterogeneous nucleation process requires less active energy than homogeneous nucleation. Therefore Ni_3Se_4 is observed to grow on the surfaces of $MoSe_2$ to form petal-like morphology instead of separated particles which are formed by independently homogeneous nucleation. With further increasing the amounts of Ni and Se sources, Ni_3Se_4 tends to grow on the surfaces of Ni_3Se_4 petals that have already formed. As a result, $MoSe_2$–Ni_3Se_4 hybrid nanostructures with increased thickness of Ni_3Se_4 petals are observed (see the morphological evolution shown in Fig. 3).

The electrocatalytic activity of as prepared catalysts was measured using a three-electrode system in acid solution. As shown in Fig. 6a, all the onset overpotentials (i.e., the potential needed to achieve a current density of 1 mA cm^{-2}) [28] of various catalysts are small. The Mo5Ni1 sample requires the lowest onset overpotential of 128 mV for HER, while for other catalysts, the values of onset overpotential are 163, 140, 162, and 216 mV for $MoSe_2$, Mo2Ni1, Mo1Ni1, and Ni_3Se_4, respectively. When cathode current density reaches -10 mA cm^{-2}, the Mo2Ni1 sample requires the smallest overpotential of 203 mV. The needed overpotentials are 234, 220 250, and 299 mV for $MoSe_2$, Mo5Ni1, Mo1Ni1, and Ni_3Se_4, respectively. To further investigate the obtained samples, the linear portions of the Tafel curves were analyzed using the Tafel equation:

$$\eta = b \log j + a \tag{1}$$

where j is the current density, η is the overpotential, and b is the Tafel slope. As can be seen in Fig. 6b, the Mo2Ni1 sample has a Tafel slope of 57 mV per decade. This value is substantially smaller than the slopes of Mo5Ni1 (85 mV per decade), Mo1Ni1 (88 mV per decade), Ni_3Se_4 (82 mV per decade) and $MoSe_2$ (71 mV per decade) samples. Meanwhile, the Pt/C exhibits a Tafel slope of ~ 33 mV per decade, corresponding well to the known values [29]. Theoretically, the lower Tafel slope suggests the faster HER kinetics [30]. The principal reaction mechanism in the HER process can be revealed by the Tafel slope [15, 19]. There are three main steps can participate in the HER process, i.e., Volmer reaction: H^+ (aq) + e^- → H_{ads}, Heyrovsky reaction: H_{ads} + H^+ (aq) + e^- → H_2 (g), and Tafel reaction H_{ads}

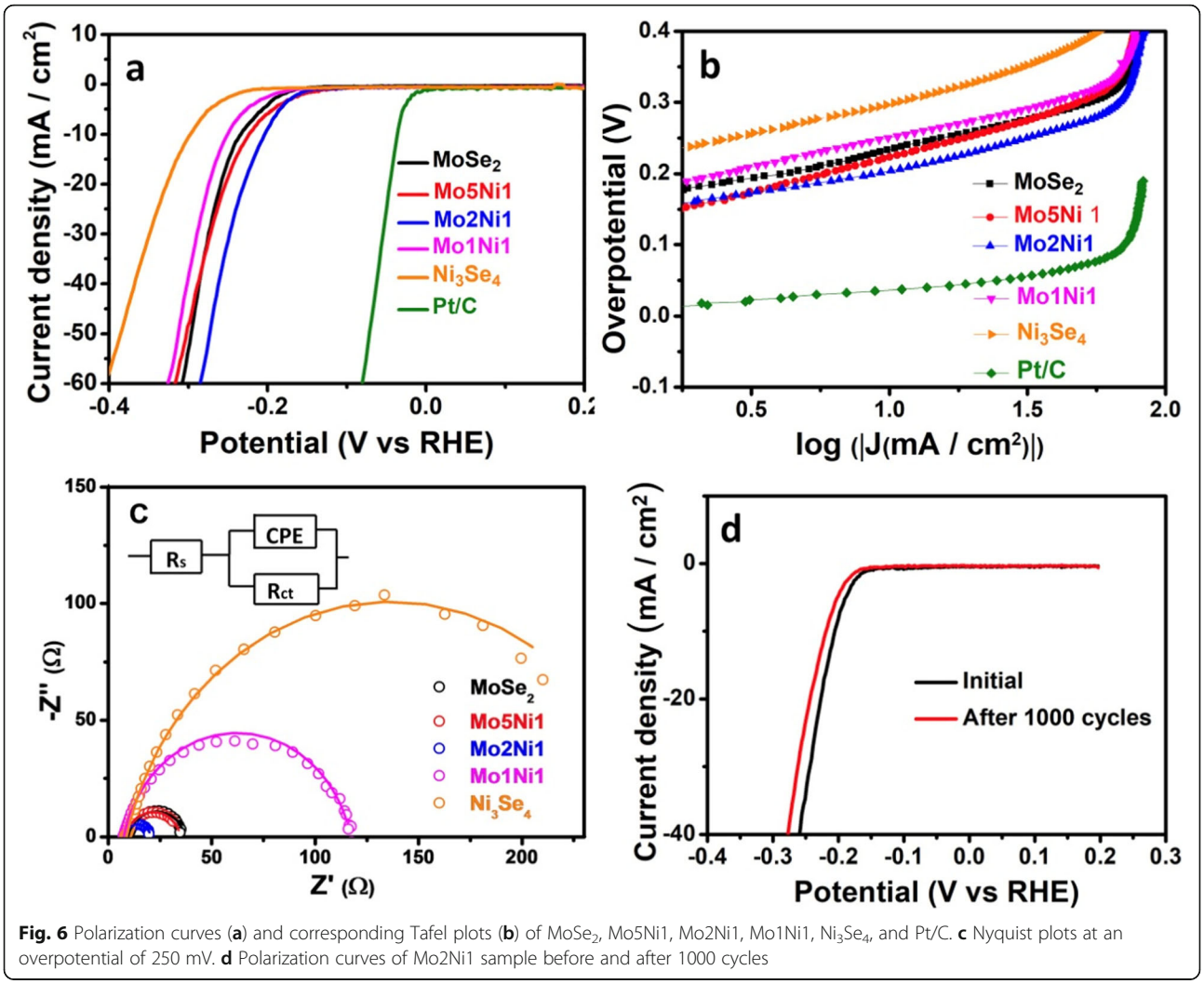

Fig. 6 Polarization curves (**a**) and corresponding Tafel plots (**b**) of $MoSe_2$, Mo5Ni1, Mo2Ni1, Mo1Ni1, Ni_3Se_4, and Pt/C. **c** Nyquist plots at an overpotential of 250 mV. **d** Polarization curves of Mo2Ni1 sample before and after 1000 cycles

+ $H_{ads} \rightarrow H_2$ (g). At 25 °C, The Tafel slope values of the three reactions are 118 mV per decade, 39 mV per decade, and 29 mV per decade, respectively [19]. Accordingly, the results in our study suggest that the mechanism of Volmer–Heyrovsky [31–33] should be dominant for all prepared samples in the HER.

In order to further investigate the kinetics of electrodes, the Nyquist plots of five samples acquired by EIS are shown in Fig. 6c. The charge transfer resistance (R_{ct}) which is achieved from the region of low frequency has a close relationship to the kinetics of electrodes. A smaller value of R_{ct} is relevant to a higher reaction rate [34]. The value of R_{ct} of Mo2Ni1 is 13.0 Ω, which is the lowest value among the five samples. For other samples, the R_{ct} values are 27.5, 27.1, 109.1, and 254.6 Ω for $MoSe_2$, Mo5Ni1, Mo1Ni1, and Ni_3Se_4, respectively. The lowest R_{ct} of Mo2Ni1 suggests the fastest charge transfer process among the as prepared samples. The result further proves the excellent HER electrocatalytic efficiency of the Mo2Ni1 sample. The better conductivity might be resulted from the modulation of electronic structure via the synergetic effects between $MoSe_2$ and Ni_3Se_4. Fig. 6d presents the polarization curves to characterize the stability of Mo2Ni1 sample. After 1000 cycles, the catalytic performance only shows a slight decline. The synergetic effects play an important in controlling the adsorptive-absorptive interactions on the catalytic surfaces and thus determine the rate determining step of the catalytic reaction [35]. Therefore, the utilization of synergetic effects constitutes a major advantage of hybrid nanostructure for the enhancement of HER activity.

To roughly calculate the electrochemically active surface area (ESCA) of the catalysts, electrochemical double-layer capacitances (C_{dl}) are measured using cyclic voltammetry (CV) at different scan rates (Additional file 1: Figure S4). The plots of $\Delta j = (j_a - j_c)$(j_a and j_c are the current density when charging and discharging at a voltage of 0.15 V, respectively) against the scan rate are shown in Fig. 7a, and the C_{dl} values are counted to be half of the slopes. Mo2Ni1 exhibits a C_{dl} value of 2.67

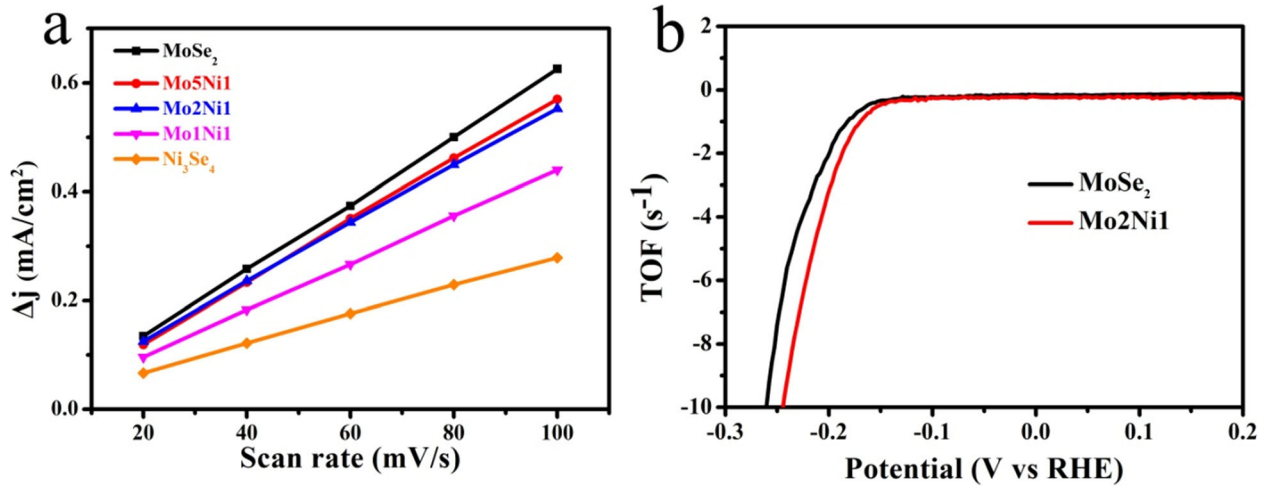

Fig. 7 **a** Double-layer capacity current versus scan rate of $MoSe_2$, Mo5Ni1, Mo2Ni1, Mo1Ni1, and Ni_3Se_4 samples. **b** Calculated TOFs of pure $MoSe_2$ and Mo2Ni1 samples

mF cm^{-2} which is slightly smaller than the value (3.06 mF cm^{-2}) of $MoSe_2$ and Mo5Ni1 (2.82 mF cm^{-2}), suggesting that the addition of Ni_3Se_4 cannot further increase the electrochemical active surface area, and the consequence is consistent with the TEM observation. Hence the reason for the improvement of the HER catalytic activity of Mo2Ni1 sample is not likely due to the increase of electrochemically active surface area but the synergistic effect between $MoSe_2$ and Ni_3Se_4, along with the promoting of conductivity. In addition, we estimated the numbers of active sites and turnover frequencies (TOFs) of various catalysts. The numbers of actives are obtained by the CV curves of different catalysts which are recorded from − 0.4 to 0.6 V in a phosphate buffer saline electrolyte with a scan rate of 50 mV s^{-1}(Additional file 1: Figure S5) [30, 36]. The calculated number of active sites for Mo2Ni1 is 1.02 × 10^{-6} mol while that for $MoSe_2$ is 0.77 × 10^{-6} mol. In addition, the calculated TOF at − 200 mV for each active site of Mo2Ni1 is 3.4 s^{-1}, which is also larger than that (2.1 s^{-1}) of $MoSe_2$ (Fig. 7b). Theoretically, the HER activity of catalysts can be attributed to three factors: (a) the active site numbers, (b) the active site quality (turnover frequency), and (c) the conductivity among active sites [37]. In this work, although Mo2Ni1 has a slightly smaller value of C_{dl} compared to $MoSe_2$, it possesses the lowest charge–transfer impedance, the most active sites and the highest TOF. Therefore, it exhibits the best overall HER activity.

Conclusions

A seed-induced solution route has been developed for the synthesis of $MoSe_2$–Ni_3Se_4 hybrid nanoelectrocatalysts. $MoSe_2$ seeds with a flower-like morphology that is composed by the assembly of ultrathin nanoflakes have been used to induce the growth of Ni_3Se_4 on the flower petals of $MoSe_2$. The chemical composition of $MoSe_2$–Ni_3Se_4 hybrid nanoelectrocatalysts can be modulated by adjusting the content of Ni_3Se_4. It has been observed that the combination of Ni_3Se_4 with $MoSe_2$ to form a hybrid nanostructure can improve the HER performances of $MoSe_2$. The $MoSe_2$–Ni_3Se_4 hybrid nanoelectrocatalyst with a Mo:Ni ratio of 2:1 delivers remarkable HER performances that have a small onset overpotential of 140 mV, an overpotential of 201 mV at 10 mA cm^{-2} and a small Tafel slope of 57 mV dec^{-1} under acidic condition. The improved conductivity and TOF have also been observed.

Supplementary information

Supplementary information accompanies this paper at https://doi.org/10.1186/s11671-020-03368-z.

Additional file 1: Fig. S1 SAED patterns of Mo5Ni1 (a), Mo2Ni1 (b) and Mo1Ni1 (c) samples. The indexes in white correspond to Ni_3Se_4 while those of red correspond to $MoSe_2$. **Fig. S2** SEM image (a) and TEM image (b) of pure $MoSe_2$. **Fig. S3** TEM images of Mo2Ni1 sample obtained using different injection rates. (a) 3.3 mL/min. (b) 1.65 mL/min. (c) XRD patterns (The bottom pattern corresponds to an injection rate of 1.65 mL/min while the up one to 3.3 mL/min). **Fig. S4** Cyclic voltammetry curves of pure (a) $MoSe_2$, (b) Mo5Ni1, (c) Mo2Ni1, (d) Mo1Ni1 and (e) pure Ni_3Se_4 in the region of 0.1 ~ 0.2 V vs RHE. **Fig. S5** Cyclic voltammograms (-0.1~0.6 V vs RHE) recorded in pH = 7 phosphate buffer.

Abbreviations

HER: Hydrogen evolution reaction; XRD: X-ray diffraction; TMDs: Transition metal dichalcogenides; SEM: Scanning electron microscopy; TEM: Transmission electron microscopy; SAED: Selected area electron diffraction; HAADF: High-angle annular dark-field; XPS: X-ray photoelectron spectroscopy; EIS: Electrochemical impedance spectroscopy; TOFs: Turnover frequencies; R_{ct}: Charge transfer resistance; C_{dl}: Electrochemical double-layer capacitances

Acknowledgements

Not applicable

Authors' Contributions
WP: Synthesis and original draft preparation; GS: Characterization and draft modifying; YC: Experiment design, writing and supervision; WX: TEM investigation; HZ: TEM investigation; JX: Supervision and data analyses; LW: Property measurement; DLP: Supervision and reviewing. The author(s) read and approved the final manuscript.

Funding
This work was supported by the National Key R&D Program (grant no. 2016YFA0202600), and the "Double-First Class" Foundation of Materials and Intelligent Manufacturing Discipline of Xiamen University.

Availability of Data and Materials
Not applicable.

Competing Interests
The authors declare that they have no competing interests.

Received: 30 March 2020 Accepted: 9 June 2020
Published online: 16 June 2020

References

1. Chen YX, Yang KN, Jiang B, Li JX, Zeng MQ, Fu L (2017) Emerging two-dimensional nanomaterials for electrochemical hydrogen evolution. J Mater Chem A 5(18):8187–8208
2. Wang Y, Kong B, Zhao D, Wang H, Selomulya C (2017) Strategies for developing transition metal phosphides as heterogeneous electrocatalysts for water splitting. Nano Today 15:26–55
3. Jing S, Zhang L, Luo L, Lu J, Yin S, Shen PK, Tsiakaras P (2018) N-doped porous molybdenum carbide nanobelts as efficient catalysts for hydrogen evolution reaction. Appl Catal B Environ 224:533–540
4. Barman BK, Das D, Nanda KK (2017) Facile and one-step synthesis of a free-standing 3D MoS_2-rGO/Mo binder-free electrode for efficient hydrogen evolution reaction. J Mater Chem A 5(34):18081–18087
5. Lai FL, Yong DY, Ning XL, Pan BC, Miao YE, Liu TX (2017) Bionanofiber assisted decoration of few-layered $MoSe_2$ nanosheets on 3D conductive networks for efficient hydrogen evolution. Small 13(7):1602866
6. Lukowski MA, Daniel AS, Meng F, Forticaux A, Li L, Jin S (2013) Enhanced hydrogen evolution catalysis from chemically exfoliated metallic MoS_2 nanosheets. J Am Chem Soc 135(28):10274–10277
7. Chen L, Zhang X, Jiang W, Zhang Y, Huang L, Chen Y, Yang Y, Li L, Hu J (2018) In situ transformation of Cu_2O@MnO_2 to Cu@$Mn(OH)_2$ nanosheet-on-nanowire arrays for efficient hydrogen evolution. Nano Res 11(4):1798–1809
8. Huang Y, Miao Y-E, Fu J, Mo S, Wei C, Liu T (2015) Perpendicularly oriented few-layer $MoSe_2$ on SnO_2 nanotubes for efficient hydrogen evolution reaction. J Mater Chem A 3(31):16263–16271
9. Mao S, Wen Z, Ci S, Guo X, Ostrikov KK, Chen J (2015) Perpendicularly oriented $MoSe_2$ /graphene nanosheets as advanced electrocatalysts for hydrogen evolution. Small 11(4):414–419
10. Yang J, Wang C, Ju H, Sun Y, Xing S, Zhu J, Yang Q (2017) Integrated quasiplane heteronanostructures of $MoSe_2$/Bi_2Se_3 hexagonal nanosheets: synergetic electrocatalytic water splitting and enhanced supercapacitor performance. Adv Funct Mater 27(48):1703864
11. Qu B, Yu XB, Chen YJ, Zhu CL, Li CY, Yin ZX, Zhang XT (2015) Ultrathin $MoSe_2$ nanosheets decorated on carbon fiber cloth as binder-free and high-performance electrocatalyst for hydrogen evolution. ACS Appl Mater Interfaces 7(26):14170–14175
12. Voiry D, Salehi M, Silva R, Fujita T, Chen M, Asefa T, Shenoy VB, Eda G, Chhowalla M (2013) Conducting MoS_2 nanosheets as catalysts for hydrogen evolution reaction. Nano Lett 13(12):6222–6227
13. Li H, Tan Y, Liu P, Guo C, Luo M, Han J, Lin T, Huang F, Chen M (2016) Atomic-sized pores enhanced electrocatalysis of TaS_2 nanosheets for hydrogen evolution. Adv Mater 28(40):8945–8949
14. Merki D, Hu X (2011) Recent developments of molybdenum and tungsten sulfides as hydrogen evolution catalysts. Energy Environ Sci 4(10):3878–3888
15. Zhang L, Wang T, Sun L, Sun Y, Hu T, Xu K, Ma F (2017) Hydrothermal synthesis of 3D hierarchical $MoSe_2$/$NiSe_2$ composite nanowires on carbon fiber paper and their enhanced electrocatalytic activity for the hydrogen evolution reaction. J Mater Chem A 5(37):19752–19759
16. Mu CH, Qi HX, Song YQ, Liu ZP, Ji LX, Deng JG, Liao YB, Scarpa F (2016) One-pot synthesis of nanosheet-assembled hierarchical $MoSe_2$/$CoSe_2$ microcages for the enhanced performance of electrocatalytic hydrogen evolution. RSC Adv 6(1):23–30
17. Wang CQ, Zhang P, Lei JL, Dong W, Wang JH (2017) Integrated 3d $MoSe_2$@$Ni_{0.85}Se$ nanowire network with synergistic cooperation as highly efficient electrocatalysts for hydrogen evolution reaction in alkaline medium. Electrochim Acta 246:712–719
18. Zhou X, Liu Y, Ju H, Pan B, Zhu J, Ding T, Wang C, Yang Q (2016) Design and epitaxial growth of $MoSe_2$–NiSe vertical heteronanostructures with electronic modulation for enhanced hydrogen evolution reaction. Chem Mater 28(6):1838–1846
19. Shi Y, Zhang B (2016) Recent advances in transition metal phosphide nanomaterials: synthesis and applications in hydrogen evolution reaction. Chem Soc Rev 45(6):1529–1541
20. Peng H, Wei C, Wang K, Meng T, Ma G, Lei Z, Gong X (2017) $Ni_{0.85}Se$@$MoSe_2$ nanosheet arrays as the electrode for high-performance supercapacitors. ACS Appl Mater Interfaces 9(20):17068–17075
21. Zhou H, Yu F, Huang Y, Sun J, Zhu Z, Nielsen RJ, He R, Bao J, Goddard WA III, Chen S, Ren Z (2016) Efficient hydrogen evolution by ternary molybdenum sulfoselenide particles on self-standing porous nickel diselenide foam. Nat Commun 7:12765
22. Guo W, Chen Y, Wang L, Xu J, Zeng D, Peng D-L (2017) Colloidal synthesis of $MoSe_2$ nanonetworks and nanoflowers with efficient electrocatalytic hydrogen-evolution activity. Electrochim Acta 231:69–76
23. Du J, Zou Z, Liu C, Xu C (2018) Hierarchical Fe-doped Ni_3Se_4 ultrathin nanosheets as an efficient electrocatalyst for oxygen evolution reaction. Nanoscale 10(11):5163–5170
24. Liu Y-R, Hu W-H, Li X, Dong B, Shang X, Han G-Q, Chai Y-M, Liu Y-Q, Liu C-G (2016) One-pot synthesis of hierarchical Ni_2P/MoS_2 hybrid electrocatalysts with enhanced activity for hydrogen evolution reaction. Appl Surf Sci 383:276–282
25. Vikraman D, Hussain S, Karuppasamy K, Feroze A, Kathalingam A, Sanmugam A, Chun SH, Jung J, Kim HS (2020) Engineering the novel $MoSe_2$-Mo_2C hybrid nanoarray electrodes for energy storage and water splitting applications. Appl Catal B-Environ 264(13):118531
26. Wang HT, Kong DS, Johanes P, Cha JJ, Zheng GY, Yan K, Liu NA, Cui Y (2013) $MoSe_2$ and WSe_2 nanofilms with vertically aligned molecular layers on curved and rough surfaces. Nano Lett 13(7):3426–3433
27. Chen Y, Ren Z, Fu H, Zhang X, Tian G, Fu H (2018) NiSe-$Ni_{0.85}Se$ heterostructure nanoflake arrays on carbon paper as efficient electrocatalysts for overall water splitting. Small 14(25):1800763
28. Cheng Y, Liao F, Shen W, Liu L, Jiang B, Li Y, Shao M (2017) Carbon cloth supported cobalt phosphide as multifunctional catalysts for efficient overall water splitting and zinc-air batteries. Nanoscale 9(47):18977–18982
29. Li Y, Wang Y, Pattengale B, Yin J, An L, Cheng F, Li Y, Huang J, Xi P (2017) High-index faceted $CuFeS_2$ nanosheets with enhanced behavior for boosting hydrogen evolution reaction. Nanoscale 9(26):9230–9237
30. Yang J, Zhu J, Xu J, Zhang C, Liu T (2017) $MoSe_2$ nanosheet array with layered MoS_2 heterostructures for superior hydrogen evolution and lithium storage performance. ACS Appl Mater Interfaces 9(51):44550–44559
31. Ge YC, Gao SP, Dong P, Baines R, Ajayan PM, Ye MX, Shen JF (2017) Insight into the hydrogen evolution reaction of nickel dichalcogenide nanosheets: activities related to non-metal ligands. Nanoscale 9(17):5538–5544
32. Najafi L, Bellani S, Oropesa-Nuñez R, Ansaldo A, Prato M, Del Rio Castillo AE, Bonaccorso F (2018) Engineered $MoSe_2$-based heterostructures for efficient electrochemical hydrogen evolution reaction. Adv Energy Mater 8(16):1703212
33. Zhao WJ, Wang SQ, Feng CQ, Wu HM, Zhang L, Zhang JJ (2018) Novel cobalt-doped $Ni_{0.85}Se$ chalcogenides ($Co_xNi_{0.85-x}Se$) as high active and stable electrocatalysts for hydrogen evolution reaction in electrolysis water splitting. ACS Appl Mater Interfaces 10(47):40491–40499
34. Liu Y, Zhou X, Ding T, Wang C, Yang Q (2015) 3D architecture constructed via the confined growth of MoS_2 nanosheets in nanoporous carbon derived from metal-organic frameworks for efficient hydrogen production. Nanoscale 7(43):18004–18009
35. Sharma L, Halder A (2018) Synergistic effect in photoelectrochemical hydrogen evolution by RGO-supported nickel molybdenum catalysts. ChemistrySelect 3:8955–8961
36. Dai X, Du K, Li Z, Liu M, Ma Y, Sun H, Zhang X, Yang Y (2015) Co-Doped MoS_2 nanosheets with the dominant CoMoS phase coated on carbon as an

excellent electrocatalyst for hydrogen evolution. ACS Appl Mater Interfaces 7(49):27242–27253
37. Tang C, Wang W, Sun A, Qi C, Zhang D, Wu Z, Wang D (2015) Sulfur-decorated molybdenum carbide catalysts for enhanced hydrogen evolution. ACS Catal 5(11):6956–6963

Publisher's Note